Vector-Valued Image Interpolation by an Anisotropic Diffusion-Projection PDE *

Anastasios Roussos and Petros Maragos

School of ECE, National Technical University of Athens, Greece
{troussos,maragos}@cs.ntua.gr

Abstract. We propose a nonlinear image interpolation method, based on an anisotropic diffusion PDE and designed for the general case of vector-valued images. The interpolation solution is restricted to the subspace of functions that can recover the discrete input image, after an appropriate smoothing and sampling. The proposed nonlinear diffusion flow lies on this subspace and its strength and anisotropy effectively adapt to the local variations and geometry of image structures. The derived model efficiently reconstructs the real image structures, leading to a natural interpolation, with reduced blurring, staircase and ringing artifacts of classic methods. This method also outperforms other existing PDE-based interpolation methods. We present experimental results that prove the potential and efficacy of the method as applied to graylevel and color images.

1 Introduction

Image interpolation is among the fundamental image processing problems and is often required for various image analysis operations. It is therefore of interest for many applications such as biomedical image processing, aerial and satellite imaging, text recognition and high quality image printing. In this paper, the term *image interpolation* is used in the sense of the operation that takes as input a discrete image and recovers a continuous image or a discrete one with higher resolution. The case where the output image is discrete appears in the literature with several other names: *digital zooming*, *image magnification*, *upsampling*, *resolution enhancement*.

There exists a large variety of image interpolation methods, which can be classified to two main classes, linear and nonlinear methods (see [1] for a detailed review). The *linear* methods (e.g. bicubic, quadratic and spline interpolations) perform convolution of the image samples with a single kernel, equivalent to a lowpass filtering. These methods yield relatively efficient and fast algorithms, but they cannot effectively reconstruct the high-frequency part of images and inevitably introduce artifacts. *Nonlinear* methods perform a processing adapted to the local geometric structure of the image, with main goal to efficiently reconstruct image edges. This class includes variational (e.g. [2–4]) and PDE-based

* Work supported by the European research program ASPI (IST-FP6-021324).

(e.g. [5, 6]) methods, some of which will be presented in the following sections. Such methods (e.g. [7–9]) have also been developed for two closely related problems, image inpainting [10] and scattered data interpolation.

In this paper a novel nonlinear method for the interpolation of vector-valued images is proposed. We pose a constraint, which effectively exploits the available information of input image. Then, we design an anisotropic diffusion PDE, which performs adaptive smoothing but also complies with this constraint, thanks to an appropriate projection operation. The diffusion strength and anisotropy adapt to the local variations and geometry of image structures. This method yields a plausible result even when the resolution of input image is relatively low and reduces the artifacts that usually appear in image interpolation. The paper is organized as follows: In Sect. 2, some interpolation models related to the proposed method are discussed. Sect. 3 presents our novel interpolation PDE model. In Sect. 4, we demonstrate results from interpolation experiments, that show the potential and efficacy of the new method.

2 Preliminaries and Background

2.1 Reversibility Condition Approach to Interpolation

The problem of image interpolation is viewed here in a way similar to [2, 3]. The continuous solution of interpolation $u(x, y)$ should yield the known, low resolution discrete image $z[i, j]$, after a lowpass filtering followed by sampling. To pose this *reversibility condition* formally, let us consider that $z[i, j]$ is defined on an orthogonal grid of $N_x \times N_y$ points with vertical and horizontal steps h_x and h_y respectively. Also let $u(x, y)$ be defined in the domain $\Omega = [\frac{h_x}{2}, N_x + \frac{h_x}{2}] \times [\frac{h_y}{2}, N_y + \frac{h_y}{2}]$, which contains the grid points. Then, the reversibility condition for the solution $u(x, y)$ can be written as follows:

$$(S * u)(ih_x, jh_y) = z[i, j]\,, \text{ for all } (i, j) \in \{1,..,N_x\} \times \{1,..,N_y\}\ , \qquad (1)$$

where h_x, h_y are hereafter considered unitary ($h_x = h_y = 1$), "$*$" denotes convolution and $S(x, y)$ is a smoothing kernel that performs the lowpass filtering and has Fourier transform with nonzero values for all the baseband frequencies $(\omega_1, \omega_2) \in [-\pi, \pi]^2$. For example, $S(x, y)$ could be the *mean kernel*, i.e. $S(x, y) = \mathbb{1}_{[-\frac{1}{2}, \frac{1}{2}]^2}(x, y)$, where $\mathbb{1}_B$ denotes the indicator function for any set $B \subset \mathbb{R}^2$. Note that (1) degenerates to the exact interpolation condition when $S = \delta(x, y)$ (2D unit impulse). However, condition (1) with an appropriate lowpass filtering can be more realistic, as it can better model the digitization process, which is the final step of image acquisition systems [4]. In addition, this lowpass filtering is desirable, as it reduces the aliasing effects at the acquired image. The problem of finding $u(x, y)$ in (1) is ill-posed, as (1) is satisfied by infinitely many functions. Let $\mathcal{U}_{z,S}$ be the set of these functions. It is easy to see that $\mathcal{U}_{z,S}$ is an affine subspace of the functions defined in Ω. Therefore, some extra criterion must be posed to choose among the functions of $\mathcal{U}_{z,S}$.

A simple linear interpolation method arises by imposing the additional constraint that $u(x, y)$ is a bandpass 2D signal, similarly to Shannon's theory. Then, the solution of (1), which we refer to as *(frequency) zero-padding interpolation*, is unique and can be easily derived using the Sampling theorem (note that it depends on the kernel $S(x, y)$). This method reconstructs image edges without blurring or distorting them, but usually introduces strong oscillations around edges [3]. The cutoff of high frequencies is thus undesirable, as the bandlimited assumption is not true for most real-world images. Therefore, a more appropriate method of selection among the functions of $\mathcal{U}_{z,S}$ is needed. Such methods will be presented in the following sections.

Total Variation Based Interpolation. Guichard and Malgouyres [2, 3] proposed to choose as solution of the interpolation the image that minimizes the Total Variation (TV), $E[u] = \iint_\Omega \|\nabla u\| \, \mathrm{d}x\mathrm{d}y$, under the constraint that $u \in \mathcal{U}_{z,S}$. This minimization problem is solved in [2] by applying a constrained gradient descent flow, described by the following PDE:

$$\partial u(x, y, t)/\partial t = P_{\mathcal{U}_{0,S}} \left\{ \mathrm{div} \left(\nabla u / \|\nabla u\| \right) \right\} \quad , \tag{2}$$

supplemented with the initial condition that $u(x, y, 0)$ is the zero-padding interpolation of $z[i, j]$. $P_{\mathcal{U}_{0,S}}\{\cdot\}$ denotes the operator of orthogonal projection on the subspace $\mathcal{U}_{0,S}$, which corresponds to the condition (1) with $z[i, j] = 0$ for all (i, j). This projection ensures that $u(x, y, t) \in \mathcal{U}_{z,S}, \forall t > 0$, since $u(x, y, 0) \in \mathcal{U}_{z,S}$. The authors propose two options for the smoothing kernel of condition (1): the mean kernel and the *sinc kernel*, which provides an ideal lowpass filter as its Fourier transform is $\mathbb{1}_{[-\pi,\pi]^2}(\omega_1, \omega_2)$.

This method leads to reconstructed images without blurring effects, as it allows discontinuities and preserves 1D image structures. However, TV minimization is based on the assumption that the desirable image is almost piecewise constant, which yields a result with over-smoothed homogeneous regions. In addition, the diffusion in (2) is controlled by the simple coefficient $1/\|\nabla u\|$, therefore it cannot remove block effects, especially in the regions with big image variations. Further, the mean kernel vanishes too sharply, so the projection $P_{\mathcal{U}_{0,S}}\{\cdot\}$ reintroduces block effects and the sinc kernel is badly localized in space and oscillates, so $P_{\mathcal{U}_{0,S}}\{\cdot\}$ causes formation of oscillations in reconstructed edges.

Belahmidi-Guichard (BG) Method. Belahmidi and Guichard [5] have improved the TV-based interpolation by developing a nonlinear anisotropic PDE, hereafter referred as *BG interpolation method*. In order to enhance edge preservation, this PDE performs a diffusion with strength and orientation adapted to image structures. The reversibility condition (1) is taken into account (with the choice of mean kernel for $S(x, y)$) by adding to the PDE an appropriate fidelity term, so that the flow $u(x, y, t)$ stays close to the subspace $\mathcal{U}_{z,S}$ (see [5] for details). This method balances linear zooming on homogeneous regions and anisotropic diffusion near edges, trying to combine the advantages of these

two processes. Nevertheless, the diffusion is not always desirably adapted to real image structures and the fact that the PDE flow is not constrained to lie inside $\mathcal{U}_{z,S}$ may decrease the accuracy of the result.

2.2 PDE Model of Tschumperlé and Deriche (TD)

Tschumperlé and Deriche [11, 6] proposed an effective PDE method for vector-valued image regularization. This PDE scheme, which we refer to as *TD PDE*, is mainly designed for image restoration applications, but it is presented here because we utilize it to the design of the new interpolation PDE (Sect. 3). Their model is an anisotropic diffusion flow, which uses tensors to adapt the diffusion to the image structure. Let $\boldsymbol{u}(x,y,t)=[u_1,..,u_M]^{\mathrm{T}}$ be the output vector-valued image at time t and M be the number of vector components. Then, the TD PDE model can be described by the following set of coupled PDEs:

$$\frac{\partial u_m(x,y,t)}{\partial t} = \mathrm{trace}\Big(T\big(J_\rho(\nabla \boldsymbol{u}_\sigma)\big)\cdot D^2 u_m\Big)\,,\; m=1,..,M \;\;, \tag{3}$$

with initial condition that $\boldsymbol{u}(x,y,0)$ is the input vector-valued image. D^2u_m denotes the spatial Hessian matrix of the component $u_m(x,y,t)$ and T is the 2×2 *diffusion tensor*:

$$T\big(J_\rho(\nabla \boldsymbol{u}_\sigma)\big) = \big[1+(\mathcal{N}/K)^2\big]^{-\frac{1}{2}}\cdot \boldsymbol{w}_-\boldsymbol{w}_-^{\mathrm{T}} \;+\; \big[1+(\mathcal{N}/K)^2\big]^{-1}\cdot \boldsymbol{w}_+\boldsymbol{w}_+^{\mathrm{T}} \;\;, \tag{4}$$

where $\mathcal{N}=\sqrt{\lambda_+ + \lambda_-}$ and K is a threshold constant similar to the diffusivity of [12].[1] Also, $\lambda_-\leq\lambda_+$ and $\boldsymbol{w}_-,\boldsymbol{w}_+$ are the eigenvalues and unit eigenvectors of the 2×2 *structure tensor*:

$$J_\rho(\nabla \boldsymbol{u}_\sigma) = G_\rho * \sum_{m=1}^{M} \nabla(G_\sigma * u_m)\;\big(\nabla(G_\sigma * u_m)\big)^{\mathrm{T}} \;\;. \tag{5}$$

The 2D isotropic Gaussian kernels G_σ and G_ρ are of standard deviation σ and ρ respectively.[2] The structure tensor $J_\rho(\nabla \boldsymbol{u}_\sigma)$ measures the local geometry of image structures (convolutions with G_σ,G_ρ make this measure more coherent [13]). The eigenvectors $\boldsymbol{w}_-$ and $\boldsymbol{w}_+$ describe the orientation of minimum and maximum vectorial variation of $\boldsymbol{u}$ and the eigenvalues λ_- and λ_+ describe measures of these variations (the term $\mathcal{N}$ is an edge-strength predictor which effectively generalizes the norm $\|\nabla u\|$). Thus, the diffusion is strong and isotropic in homogenous regions (small $\mathcal{N}$), but weak and mainly oriented by image structures near the edges (big $\mathcal{N}$). Consequently, this method offers a flexible and effective control on the diffusion process (see [6] for more details).

[1] This is a slightly more general version of the original model [11, 6], where $K=1$.
[2] The original model corresponds to σ=0 but we use the more general version of [13].

Application to the Interpolation. Among various applications, the generic PDE model (3) of [11, 6] is applied to image interpolation (we refer to the derived method as *TD interpolation method*). This method casts image interpolation as a special case of the image inpainting problem [10]. It imposes the constraint that the solution must coincide with the input at the appropriate pixels in the new coarser grid (exact interpolation condition). Thus, the inpainting domain (i.e. the domain where the image values are unknown) consists of the remaining pixels. The image values in this domain are processed according to PDE (3), with a modified diffusion tensor [11]:

$$T\big(J_\rho(\nabla \boldsymbol{u}_\sigma)\big) = \left[1 + (\mathcal{N}/K)^2\right]^{-\frac{1}{2}} \cdot \boldsymbol{w}_- \boldsymbol{w}_-^{\mathrm{T}} \ . \tag{6}$$

The bilinear interpolation of the input image is chosen as initial condition $\boldsymbol{u}(x, y, 0)$ and the interpolation solution is derived from the equilibrium state. Contrary to the effectiveness of the TD PDE model for image restoration, the derived interpolation method suffers from some inefficiencies. The initialization by the bilinear interpolation contains edges with significant blurring. Also, the information of each input value $z[i, j]$ is not spread to all the corresponding pixels of the coarser grid, as some pixels stay anchored whereas the rest pixels change without constraint. Furthermore, the diffusion tensor (6) is fully anisotropic even in regions with small image variations, therefore it may distort image structures and create false edges.

3 The Proposed Anisotropic Diffusion-Projection PDE

The aforementioned PDE interpolation methods outperform classic linear methods, as they reconstruct the edges without blurring them. In some cases though, they yield artifacts such as over-smoothing of homogeneous regions, block effects or edge distortion. In order to improve the effectiveness of these methods, we propose a novel PDE model, which performs a nonlinear interpolation. It is based on an efficient combination of the reversibility condition approach and TD PDE (3). The model is designed to deal with vector-valued images in general and processes the different channels in a coupled manner.

More precisely, the design of our model has been based on the observation that the TV-based interpolation PDE (2) can be derived from a non-minimization point of view: it is in fact a modification of the zero-fidelity (λ=0) TV PDE [14]:

$$\partial u(x, y, t)/\partial t = \operatorname{div}\left(\nabla u / \|\nabla u\|\right) \ , \tag{7}$$

which can be viewed as a special case of the general nonlinear diffusion of [12]. This modification is done by replacing the right hand side (RHS) of the PDE with its projection to $\mathcal{U}_{0,S}$. Thanks to this projection, the whole flow remains into the subspace $\mathcal{U}_{z,S}$, provided that $u(x, y, 0) \in \mathcal{U}_{z,S}$. We followed a similar approach to design the proposed PDE model, but instead of TV PDE (7), we chose to modify the TD PDE (3), as it is an effective and robust diffusion PDE model for image regularization (see Sect. 2.2).

Before we proceed to the description of our model, let us mention that we straightforwardly generalize the condition (1) for vector-valued images: it should be satisfied independently by every channel. This generalized reversibility condition can be equivalently written as:

$$\langle S_{ij}, u_m \rangle_{L^2(\Omega)} = z_m[i,j] \ , \tag{8}$$

where $(m,i,j) \in \{1,..,M\} \times \{1,..,N_x\} \times \{1,..,N_y\}$ and $z_m[i,j]$, $u_m(x,y)$ are the m-th of M components of the discrete input and interpolated image respectively. Also, $S_{ij}(x,y) = S(i-x, j-y)$ and $\langle \cdot, \cdot \rangle_{L^2(\Omega)}$ denotes the inner product of $L^2(\Omega)$. Let $\boldsymbol{\mathcal{U}}_{z,S}$ be the set of vector-valued images $\boldsymbol{u}(x,y)$ that satisfy the generalized reversibility condition (8).

Description of the Model. We derive the interpolated image from the equilibrium solution of the following system of coupled PDEs:

$$\frac{\partial u_m(x,y,t)}{\partial t} = P_{\mathcal{U}_{0,S}} \left\{ \text{trace} \Big(T\big(J_\rho(\nabla \boldsymbol{u}_\sigma)\big) \cdot D^2 u_m \Big) \right\} \ , \ m{=}1,..,M \ , \tag{9}$$

where $P_{\mathcal{U}_{0,S}}\{\cdot\}$ denotes the operator of orthogonal projection on the subspace $\mathcal{U}_{0,S}$ and the tensors $T(J_\rho(\nabla \boldsymbol{u}_\sigma))$ and $J_\rho(\nabla \boldsymbol{u}_\sigma)$ are again given by (4) and (5) respectively. We have chosen the following initial conditions for (9): every $u_m(x,y,0)$ is derived from the zero-padding interpolation (see Sect.2.1) of the symmetrically extended $z_m[i,j]$. This initialization, which is similar to the one of PDE (2) proposed in [2], can be easily computed and contains efficient reconstructions of image edges (see also the following discussion of the model's properties). The reflection that we added before zero-padding offers a slight improvement of the initial estimate, as it eliminates the ringing effects near the image borders. Note that $\boldsymbol{u}(x,y,0) \in \boldsymbol{\mathcal{U}}_{z,S}$, so $P_{\mathcal{U}_{0,S}}\{\cdot\}$ ensures that $\boldsymbol{u}(x,y,t) \in \boldsymbol{\mathcal{U}}_{z,S}$, $\forall t > 0$.

Let us now derive an expression for the projection $P_{\mathcal{U}_{0,S}}\{\cdot\}$. First of all, the subspace $\mathcal{U}_{0,S}$ can be defined as the set of functions $v(x,y)$ that satisfy $\langle S_{ij}, v \rangle_{L^2(\Omega)} = 0$, for all $(i,j) \in \{1,..,N_x\} \times \{1,..,N_y\}$. If we assume for the chosen smoothing kernel that:

$$S(x,y) = 0 \, , \text{ for all } (x,y) \notin [-1/2, 1/2]^2 \ , \tag{10}$$

each S_{ij} takes nonzero values only inside a different square of Ω. Therefore $\langle S_{ij}, S_{i'j'} \rangle_{L^2(\Omega)} = \|S\|^2_{L^2(\mathbb{R}^2)} \, \delta_{i-i',j-j'}$ (where $\delta_{i,j}$ is the 2D discrete unit impulse), which means that the set of all S_{ij} is an orthogonal basis of $\mathcal{U}_{0,S}$. Consequently, a relatively simple expression for the projection $P_{\mathcal{U}_{0,S}}\{\cdot\}$ can be derived:

$$P_{\mathcal{U}_{0,S}}\big\{v\big\} = v - \|S\|^{-2}_{L^2(\mathbb{R}^2)} \sum_{i=1}^{N_x} \sum_{j=1}^{N_y} \langle S_{ij}, v \rangle_{L^2(\Omega)} \cdot S_{ij} \ , \tag{11}$$

The assumption (10), apart from simplifying the expression for $P_{\mathcal{U}_{0,S}}\{\cdot\}$, it is also realistic for most image acquisition systems: during the digitization process, the

measured value at any pixel (i,j) depends mainly on the intensities of points that lie in the interior of this pixel's area, i.e. the domain $\Omega_{ij} = [i-\frac{1}{2}, i+\frac{1}{2}]\times[j-\frac{1}{2}, j+\frac{1}{2}]$. Therefore we have chosen the following smoothing kernel:

$$S(x,y) = \mathbb{1}_{[-\frac{1}{2},\frac{1}{2}]^2}(x,y) \cdot \frac{G_{\hat{\sigma}}(x,y)}{\iint_{[-\frac{1}{2},\frac{1}{2}]^2} G_{\hat{\sigma}}(x',y')\mathrm{d}x'\mathrm{d}y'} \ , \tag{12}$$

where $G_{\hat{\sigma}}(x,y)$ is the 2D isotropic Gaussian of standard deviation $\hat{\sigma}$. Multiplication with $\mathbb{1}_{[-\frac{1}{2},\frac{1}{2}]^2}(x,y)$ is done to satisfy the assumption (10) and the denominator of (12) normalizes the kernel to have unitary mean value. Note that $\hat{\sigma}$ must be neither too small nor too big. If $\hat{\sigma}$ is too small, $S(x,y)$ is too localized in space and the information of each input value $z[i,j]$ is not spread properly to all the corresponding pixel area Ω_{ij}. In addition, if $\hat{\sigma}$ is too big, $S(x,y)$ reduces to the mean kernel. This kernel though is undesirable, because we want to relax the constraints near the border of each Ω_{ij} and thus prevent $P_{\mathcal{U}_{0,S}}\{\cdot\}$ from producing block effects.

Properties of the Model. As already mentioned, the zero-padding interpolation, which we use as initial condition of (9), efficiently reconstructs image edges without blurring or distorting them, but also introduces strong oscillations around edges (see [3]). It can thus be viewed as a desirable interpolation result degraded by a significant amount of noise. The scope of the proposed PDE (9) is to effectively regularize the image $\boldsymbol{u}(x,y,0)$ by removing these oscillations. Note also that (11) shows that the projection $P_{\mathcal{U}_{0,S}}\{v\}$ subtracts the component of v that does not comply with the reversibility condition. This subtraction does not affect the basic characteristics of the regularization that the velocity $v_m = \mathrm{trace}(T\cdot D^2 u_m)$ tends to apply to the image. Therefore, PDE (9) performs an anisotropic smoothing with properties very similar to (3). This fact, in combination with the analysis of Sect. 2.2, shows that the proposed PDE efficiently removes the undesirable oscillations and simultaneously preserves the important image structures. Namely, the proposed PDE can be considered as a diffusion flow towards elements of $\boldsymbol{\mathcal{U}}_{z,S}$ with "better" visual quality. Additionally, the projection $P_{\mathcal{U}_{0,S}}\{v\}$ offers the advantage that there is no need to specify the stopping time as an additional parameter. The best regularized image is derived at $t\to\infty$, where the flow equilibrates thanks to the term that $P_{\mathcal{U}_{0,S}}\{v\}$ subtracts from the velocity v.

Numerical Implementation. The continuous result $\boldsymbol{u}(x,y)$ of the proposed model is approximated by a discrete image $\boldsymbol{u}[i',j']$, defined to a coarser grid than the input image $\boldsymbol{z}[i,j]$, i.e. a discrete interpolation is performed. We consider only the case where the grid step of $\boldsymbol{z}[i,j]$ is a multiple of the grid step of $\boldsymbol{u}[i',j']$ by an integer factor d, which we call *zoom factor*. Namely, the input image is magnified $d\times d$ times. For the sake of simplicity, we hereafter assume that the coarser grid of $\boldsymbol{u}[i',j']$ has unit step, hence the grid of input $\boldsymbol{z}[i,j]$ has step d. In the discretization of PDE (9), we used an explicit numerical scheme with finite

differences, similar to [11]. The discrete time step δt was chosen sufficiently small for stability purposes (the typical value of δt=0.2 was used). Due to the fact that the output image is given at the equilibrium, we stop the iterative process when $\boldsymbol{u}^{n+1}$ differs from $\boldsymbol{u}^n$ by a small constant, with respect to an appropriate norm.

4 Experimental Results and Comparisons

In order to compare the interpolation methods and extract performance measures, we use the following protocol: We choose a reference image with a relatively good resolution and negligible noise. We reduce the dimensions of this image by an integer factor d (i.e. the image is reduced to $\frac{1}{d}\times\frac{1}{d}$ of its size), using a decimation process, i.e. (anti-aliasing) lowpass filtering followed by subsampling. We implement the lowpass filtering by a convolution with a bicubic spline, which results to a reliable and commonly used decimation process. Finally, we apply the interpolation methods to enlarge the decimated image by the zoom factor d, so that the output images have the same size as the reference image. Note that we implemented the other PDE-based interpolation methods with a way similar to the implementation of the proposed method, as briefly described in Sect. 3. Also, we used the range $[0, 255]$ for image values and in the case of color, we applied the corresponding PDE methods representing the images in the RGB color space. The reference image can be considered as the ideal output of the interpolation, as it is noiseless. Therefore the difference between the reference image $\boldsymbol{r}[i, j]$ and the output of a method $\boldsymbol{u}[i, j]$ can be viewed as reconstruction error and is quite representable of the method performance.

We use two measures for this error, the classic peak signal-to-noise-ratio (PSNR)[3] and the mean structural similarity (MSSIM) index [15], which seems to approximate the perceived visual quality of an image better than PSNR or various other measures. MSSIM index takes values in [0,1] and increases as the quality increases. We calculate it based on the code available at:
`http://www.cns.nyu.edu/~lcv/ssim/`, using the default parameters. In the case of color images, we extend MSSIM with the simplest way: we calculate the MSSIM index of each RGB channel and then take the average.

We repeat the above procedure for different reference images from a dataset and for zoom factors d=2,3 and 4. For every zoom factor and interpolation method, we compute the averages of PSNR and MSSIM for all the images in the set, which we consider as final measures of performance.

We followed the above experimental protocol using a dataset of 23 natural images of size 768×512 pixels.[4] We run two series of experiments, the first for the graylevel versions (where we applied bicubic, TV-based, BG and the proposed method) and the second for their color counterparts (where we applied bicubic, TD and our method.[5]) For the methods that needed specification of parame-

[3] We use the definition PSNR=$10\log_{10}\left(255^2 M/\text{var}\left\{\|\boldsymbol{u}[i,j]-\boldsymbol{r}[i,j]\|\right\}\right)$, where $\|\cdot\|$ denotes here the Euclidean norm of vectors with M components.

[4] The kodak collection, available from `http://www.cipr.rpi.edu/resource/stills/`.

[5] TV-based and BG methods are applicable to graylevel images only.

ter(s), we utilized fixed values in all the dataset, which we empirically derived based on a visual plausibility criterion. We have hence chosen the parameters σ=0.3d, ρ=0.4d, $\hat{\sigma}$=0.6d and K=1 for the proposed method. Also, in TD method we used the same values ρ=0.4d, K=1 and in BG method we used K=3 for the corresponding threshold constant. An extensive demonstration of these results can be found at `http://cvsp.cs.ntua.gr/~tassos/PDEinterp/ssvm07res`.

Figure 1 is a snapshot of the results for graylevel image interpolation (for the sake of demonstration, the input image has been enlarged by the simple zero order hold (ZOH)). It can be observed that the bicubic interpolation significantly blurs the edges (e.g. note the flower boundary in Fig. 1(b)). The TV-based interpolation over-smooths some homogeneous areas (e.g. the interior of the flower in Fig. 1(c)), creates block effects (e.g. the thin black branch at the upper right of Fig. 1(d)) and oscillations in reconstructed edges (e.g. the shutter behind the flower in Fig. 1(c)). BG interpolation shows an improved performance but it maintains the block effects in some regions (e.g. the flower boundary in Fig. 1(e)). Figure 1(f) shows that the proposed method yields the most effective reconstruction of image structures and the most plausible result. Observe finally how the shutter is desirably reconstructed only by the proposed method.

(a) Input (enlarged by ZOH) (b) Bicubic Interpolation (c) TV [2], sinc kernel

(d) TV [2], mean kernel (e) BG interpolation [5] (f) Proposed method

Fig. 1. Details of 4×4 graylevel interpolation using the 7$^{\text{th}}$ image of dataset.

Figure 2 demonstrates a detail of the results for interpolation in color images. We observe that bicubic interpolation gives again a result with blurring but

also significant staircase effects (e.g. note the edges of motorbikes in Fig. 2(b)). Fig. 2(c) shows that TD interpolation yields an excessively synthetic aspect to the result, as it has distorted image edges and created false thin edges around the real ones. The proposed method yields again a result (Fig. 2(d)) which has not any notable artifact and seems the most aesthetically satisfying. This result contains sharper and better localized edges than the bicubic interpolation (e.g. note the more effective reconstruction of motorbikes' edges) and looks much more natural than the result of TD interpolation.

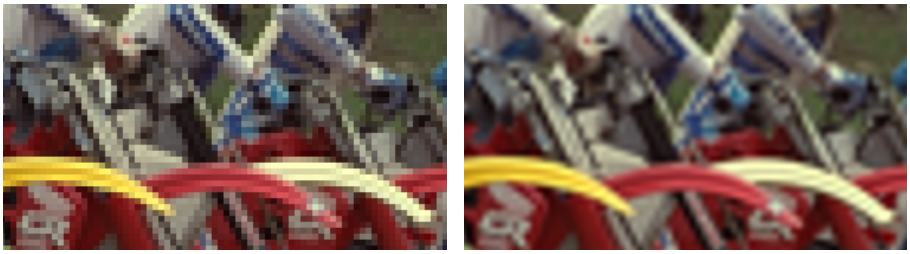

(a) Input (enlarged by ZOH) (b) Bicubic Interpolation

(c) TD interpolation [11, 6] (d) Proposed method

Fig. 2. Details of 4×4 color interpolation using the 5^{th} image of dataset.

Table 1 contains the overall performance measures of the interpolation methods, for the two series of experiments in the dataset of the 23 images. We see that the proposed method yields improved PSNR and MSSIM results in all the cases of zoom factors and series of experiments. This improvement may be attributed to the fact that the proposed method performs a more flexible adaptive smoothing and reliably exploits the input image data to increase the accuracy of the result.

Interpolation of Biomedical Vocal Tract images. In this experiment, we have used an MRI midsagittal image of a speaker's vocal tract from:
`http://www.speech.kth.se/~olov/`. Fig. 3(a) is a close-up of a denoised (using anisotropic diffusion) version of this image. Image data of this type are important for the analysis and modeling of the human speech production system. Similarly

Table 1. Average error measures in all results using the 23 images, for different zoom factors d.

Experiments with graylevel images

	Average PSNR (dB)			Average MSSIM		
Interpolation Method	d=2	d=3	d=4	d=2	d=3	d=4
Bicubic interpolation	29.14	26.68	25.55	0.8561	0.7464	0.6953
TV based [2], sinc kernel	29.75	26.87	25.94	0.8739	0.7567	0.7105
TV based [2], mean kernel	29.53	26.83	25.82	0.8714	0.7578	0.7114
BG interpolation [5]	28.36	26.58	25.60	0.8253	0.7402	0.7004
Proposed method	**30.22**	**26.96**	**26.05**	**0.8816**	**0.7671**	**0.7194**

Experiments with color images

	Average PSNR (dB)			Average MSSIM		
Interpolation Method	d=2	d=3	d=4	d=2	d=3	d=4
Bicubic interpolation	29.11	26.66	25.56	0.8524	0.7425	0.6921
TD interpolation [11]	26.77	23.89	23.37	0.7925	0.6330	0.6147
Proposed method	**30.16**	**26.96**	**26.06**	**0.8779**	**0.7631**	**0.7157**

to the above experiments, we used this image as reference and we reduced its dimensions by a factor d=3 (see Fig. 3(b)). Finally, we applied the proposed method to (3×3) interpolate the decimated image (Fig. 3(c)). We see that the proposed method yields a very satisfactory reconstruction of vocal tract shape, even though the decimated input image has notably low resolution. This simple example reveals that the proposed model can be also used to effectively enhance the resolution of medical image data of the vocal tract.

(a) Reference image (b) Input(enlarged by ZOH) (c) Proposed method

Fig. 3. Interpolation (3×3) of a vocal tract image using the proposed method.

5 Conclusions

In this paper, we have proposed a model for the interpolation of vector-valued images, based on an anisotropic diffusion PDE. Our main contribution is an efficient

combination of the reversibility condition approach [2] with the Tschumperlé-Deriche PDE model [6]. The proposed mopdel reduces the undesirable effects of classic linear and similar PDE based interpolation methods. Extensive experimental results have demonstrated the potential and efficacy of the method as applied to graylevel and color images.

Finally, we remark that the proposed PDE (9) is only one possible choice, as it is derived using the RHS of TD PDE (3), and a similar approach can be obtained using the RHS of other effective regularization PDEs. For example, based on the general anisotropic diffusion model of [13], one can use the RHS $\mathrm{div}(T{\cdot}\nabla u_m)$, with the tensor T given by (4). This method performs very similarly to the proposed method, yielding a slight improvement, as revealed by some preliminary experiments that we performed. In addition, note that the proposed model assumes that the input image is noise free. It can be modified to handle noisy inputs, if the projection operator is replaced by an appropriate fidelity term. These issues are part of our ongoing research and we plan to present them in a following paper.

References

1. Meijering, E.: A chronology of interpolation: from ancient astronomy to modern signal and image processing. Proc. IEEE **90**(3) (2002) 319–342
2. Guichard, F., Malgouyres, F.: Total variation based interpolation. In Proc. EUSIPCO **3** (1998) 1741–1744
3. Malgouyres, F., Guichard, F.: Edge direction preserving image zooming: a mathematical and numerical analysis. SIAM J. Num. Anal. **39**(1) (2001) 1–37
4. Aly, H.A., Dubois, E.: Image up-sampling using total-variation regularization with a new observation model. IEEE Tr. Im. Pr. **14**(10) (2005) 1647–1659
5. Belahmidi, A., Guichard, F.: A partial differential equation approach to image zoom. ICIP (2004) 649–652
6. Tschumperlé, D., Deriche, R.: Vector-valued image regularization with PDE's : A common framework for different applications. IEEE -PAMI **27**(4) (2005) 506–517
7. Caselles, V., Morel, J.M., Sbert, C.: An axiomatic approach to image interpolation. IEEE Tr. Im. Pr. **7**(3) (1998) 376–386
8. Chan, T.F., Shen, J.: Mathematical models for local nontexture inpaintings. SIAM J. Appl. Math. **62**(3) (2002) 1019–1043
9. Weickert, J., Welk, M.: Tensor field interpolation with PDEs. In: Visualization and Processing of Tensor Fields. Springer, Berlin (2006) 315–325
10. Bertalmio, M., Sapiro, G., Caselles, V., Ballester, C.: Image inpainting. Proc. SIGGRAPH 2000 (2000) 417–424
11. Tschumperlé, D.: PDE's Based Regularization of Multivalued Images and Applications. PhD thesis, Univ. of Nice-Sophia Antipolis (2002)
12. Perona, P., Malik, J.: Scale space and edge detection using anisotropic diffusion. IEEE -PAMI **12**(7) (1990) 629–639
13. Weickert, J.: Anisotropic Diffusion in Image Processing. Teubner, Stuttgart (1998)
14. Rudin, L., Osher, S., Fatemi, E.: Nonlinear total variation based noise removal algorithms. Physica D **60** (1992) 259–268
15. Wang, Z., Bovik, A., Sheikh, H., Simoncelli, E.: Image quality assessment: from error visibility to structural similarity. IEEE Tr. Im. Pr. **13**(4) (2004) 600–612